Cell Reports, Volume *40*

Supplemental information

RBM45 is an m^{6}A-binding protein that affects neuronal differentiation and the splicing of a subset of mRNAs

Seung H. Choi, Mathieu N. Flamand, Bei Liu, Huanyu Zhu, Meghan Hu, Melanie Wang, Jonathon Sewell, Christopher L. Holley, Hashim M. Al-Hashimi, and Kate D. Meyer

Supplemental Figure 1

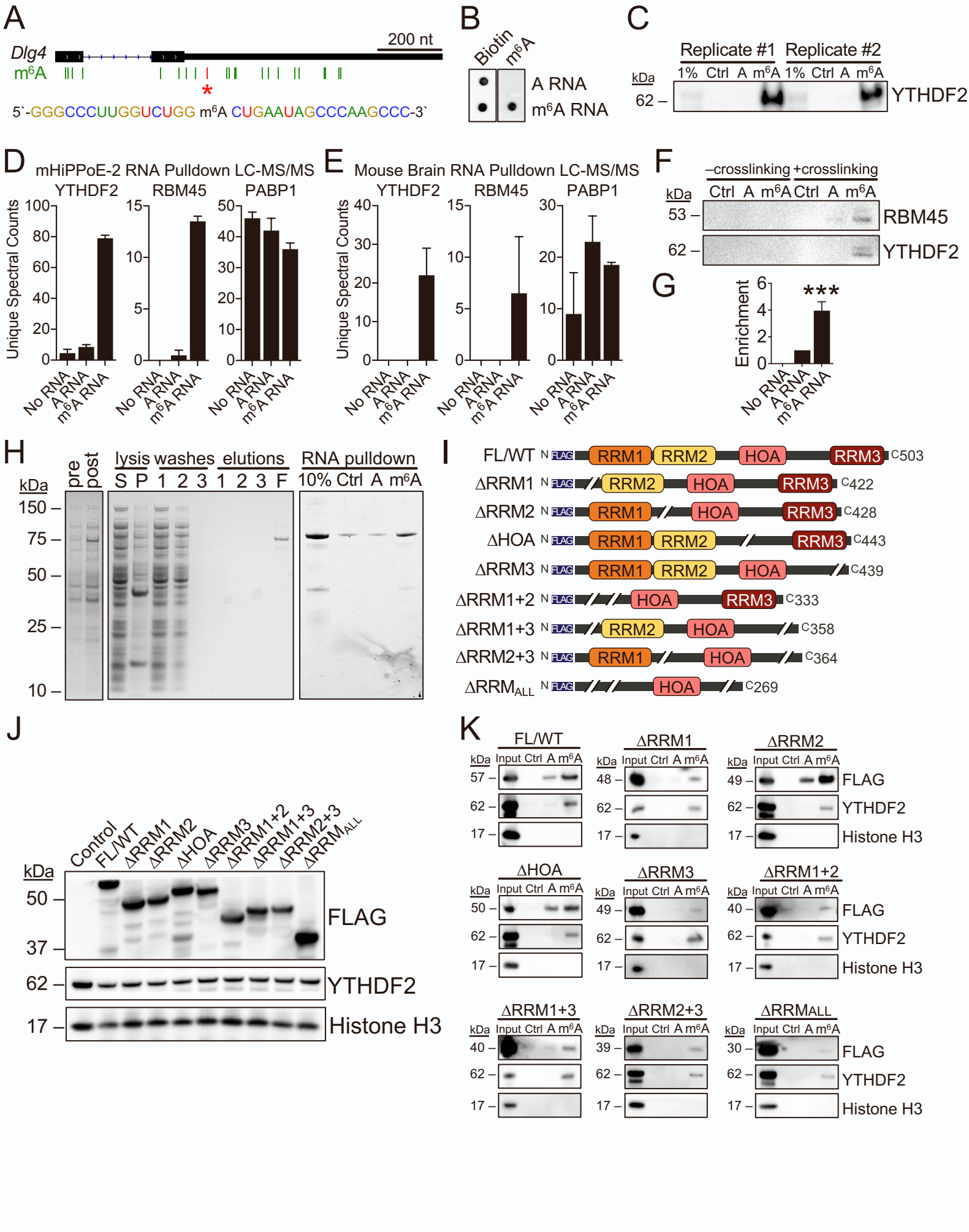

Supplementary Figure 1. Biochemical characterization of m^{6}A recognition by RBM45.

Related to Figure 1.

(A) Bait sequence for RNA pulldown-MS studies and the corresponding region within the 3'UTR of the *Dlg4* mRNA from which it was derived. m^{6}A sites identified by m^{6}A CLIP are shown in green; m^{6}A site within the bait RNA is highlighted in red (*).

(B) Dot blot confirming the presence of the biotin tag and m^{6}A in RNA baits used for RNA pulldown experiments.

(C) Western blot of eluents from RNA pulldown assays indicating binding of YTHDF2 to m^{6}A-modified RNA. Two biological replicates from RNA pulldowns using mHippoE-2 cell lysates are shown. 1%=1% of input lysate; Ctrl=pulldown performed without RNA; A=pulldown with unmodified RNA; m^{6}A=pulldown with m^{6}A-modified RNA.

(D) Unique spectral counts for YTHDF2 (positive control), RBM45 (target), and PABP1 (negative control) from RNA pulldown-MS datasets using mHippoE-2 cells. Mean ± SEM of 2 biological replicates is shown.

(E) Unique spectral counts for YTHDF2 (positive control), RBM45 (target), and PABP1 (negative control) from RNA pulldown-MS datasets using mouse brain lysates. Mean ± SEM of 2 biological replicates is shown.

(F) Western blot of eluents from RNA pulldown assays performed with and without UV crosslinking. RNA pulldowns were performed using HEK293T cell lysates, and western blots detect endogenous RBM45 and YTHDF2 (positive control). Both proteins bind directly to m^{6}A-modified RNA.

(G) Densitometry quantification of RNA pulldown assays in (F) reveals preferential binding of RBM45 to m^{6}A-modified RNA. Mean ± SEM measurements of biological replicates is plotted, n=2. Statistical significance was determined using a *Welch's* t-test.

(H) Induction and step-wise purification of GST-tagged RBM45 from BL21 bacterial cells. *Left:* Normalized amounts of pre- and post-induced whole cell bacterial extracts (0.01 OD/µL) were subjected to SDS-PAGE and Coomassie staining ("pre" and "post"). *Middle:* Soluble and insoluble fractions ("S" and "P") from cell lysates are shown, as well as eluents from washes of the RBM45-bound bead matrix and subsequent elutions. The final concentrated eluent is indicated ("F"). *Right:* RNA pulldown-Coomassie stain using *in vitro* purified GST-tagged RBM45. Input=10 µg of input protein; Ctrl=pulldown performed without RNA; A=pulldown using unmodified RNA; m^{6}A=pulldown using m^{6}A-modified RNA. Data representative of 5 biological replicates.

(I) Schematic showing the RBM45 domain deletion variants used for RNA pulldown assays in (J-K).

(J) Western blot of input lysates used for RNA pulldown assays. The indicated RBM45 variants were transfected into HEK293T cells and used for RNA pulldown assays in (K).

(K) RNA pulldown assays using A or m^{6}A-modified RNA baits were performed using lysates from HEK293T cells expressing the indicated RBM45 variants (I,J). YTHDF2 is shown as a positive control. Data are representative of four biological replicates. "Input" lanes contain 10 µg of HEK293T whole cell lysates from (J). Pulldowns were performed without RNA ("Ctrl"), with 2 µg of unmodified RNA ("A"), or with 2 µg of m^{6}A-modified RNA ("m^{6}A").

Supplemental Figure 2

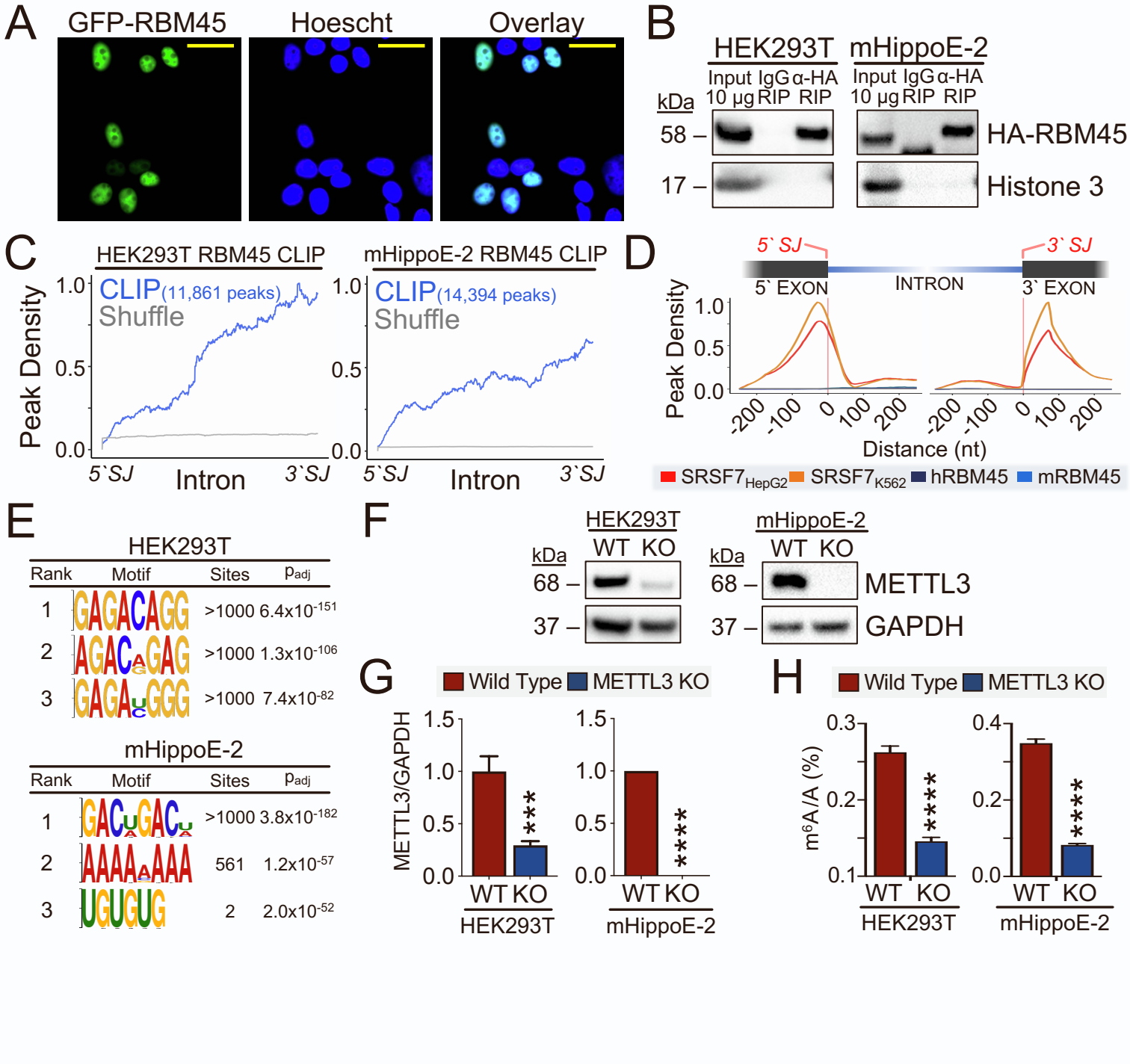

Supplementary Figure 2. RBM45 binds within introns of target transcripts.

Related to Figure 2.

(A) Exogenous RBM45 is localized predominantly to the nucleus. HEK293T cells were transfected with GFP-RBM45 followed by fluorescence imaging. Yellow scale bar=25 μm.

(B) Western Blot validation of HA RIP in mHippoE-2 and HEK293T stable cell lines expressing HA-tagged RBM45. Histone H3 is shown as a negative control. Input=10 μg of whole cell lysate; IgG RIP=eluent from control RIP using immunoglobulin (IgG); α-HA RIP=eluent from RIP using an anti-HA antibody. Data are representative of three biological replicates.

(C) Metagene profile of RBM45 CLIP peaks from mHippoE-2 and HEK293T datasets shows a preference for binding internally and near the 3' end of introns. Shuffled peak regions are shown as a control.

(D) Metagene profiles of RBM45 CLIP peaks from mHippoE-2 and HEK293T datasets around 5` and 3` exon-intron junction splice sites. RBM45 CLIP peaks are not significantly enriched within 250 nt of target transcript exon-intron junctions. Profiles of eCLIP peaks for the splicing factor SRSF7 in HepG2 cells (ENCSR513NDD) and K562 cells (ENCSR468FSW), are shown as a positive control.

(E) Top three motifs, listed by rank with the number of sites and adjusted p-values (p_{adj}) shown, enriched in RBM45 CLIP peak regions in mHippoE-2 and HEK293T cell datasets.

(F) Western blot validation of METTL3 depletion in HEK293T and mHippoE-2 stable cells.

(G) Densitometry quantification of METTL3 depletion in HEK293T and mHippoE-2 stable cells from the analysis shown in (F). Mean ± SEM from three biological replicates is plotted. Statistical significance was determined using a *Welch's* t-test; *** $p \leq 1.0 \times 10^{-4}$, **** $p \leq 1.0 \times 10^{-5}$.

(H) UPLC-MS/MS analysis of m^6A levels from purified mRNA in the indicated cell types. METTL3 depletion results in a ~50% decrease in m^6A in HEK293T cells and a ~75% decrease in mHippoE-2 cells. Mean ± SEM from three biological replicates is plotted. Statistical significance was calculated using a *Welch's* t-test; **** $p \leq 1.0 \times 10^{-5}$.

Supplemental Figure 3

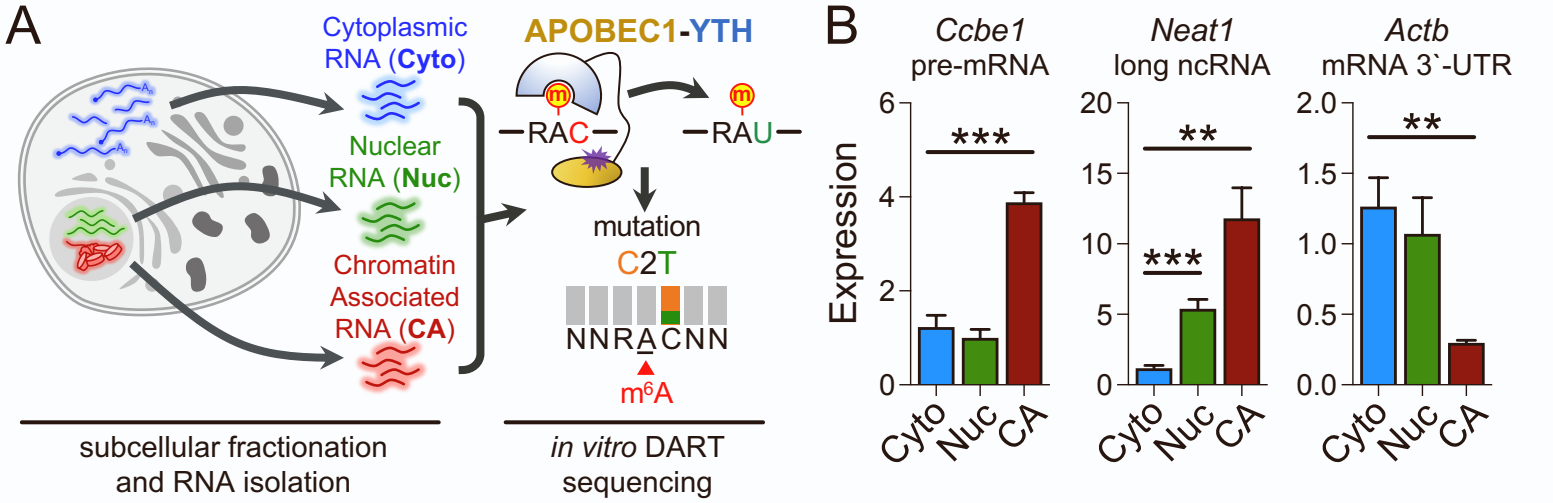

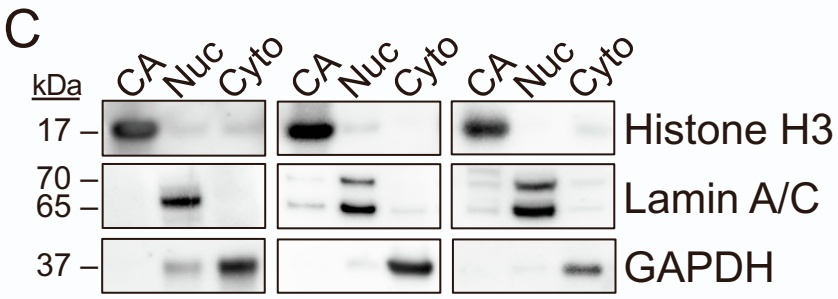

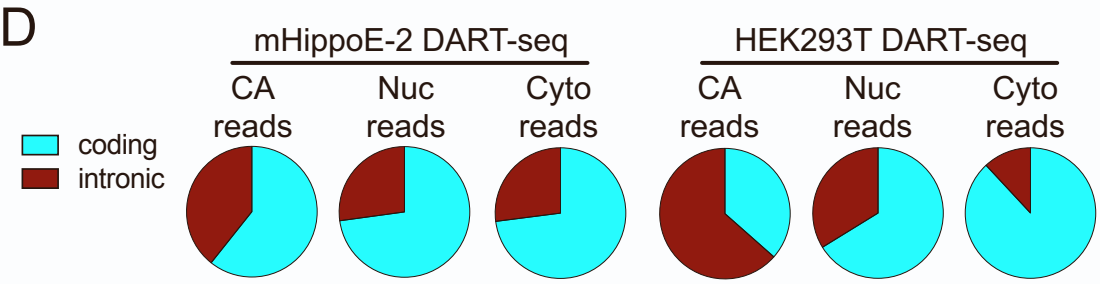

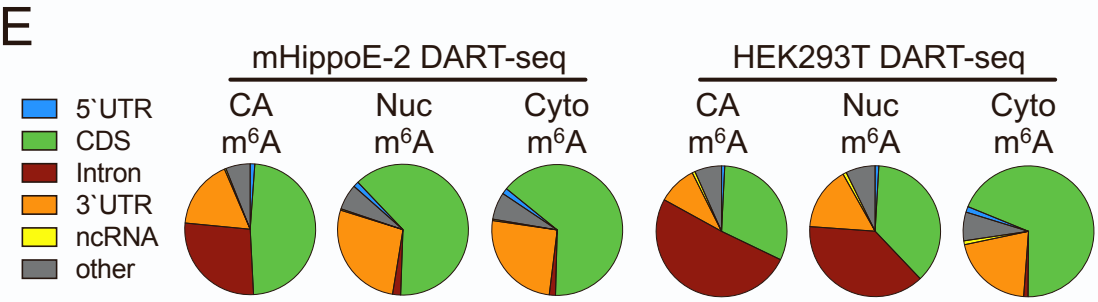

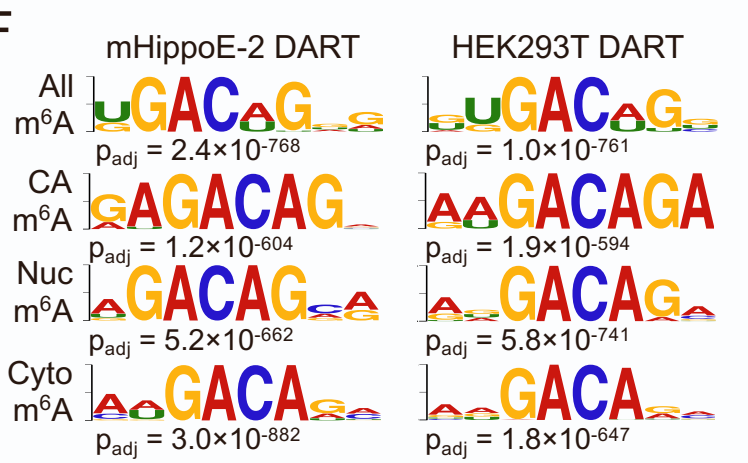

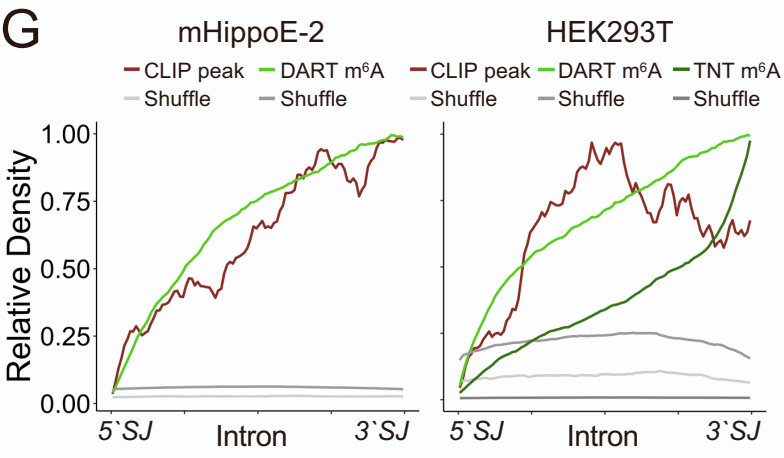

Supplementary Figure 3. Subcellular RNA fractionation and transcriptome-wide m^{6}A profiling using *in vitro* DART-seq. Related to Figure 2.

(A) Experimental workflow for isolation of subcellular RNA fractions followed by m^{6}A profiling with *in vitro* DART-seq. m^{6}A sites are identified by detecting C-to-U deamination events (C2T mutations in sequencing data) adjacent to m^{6}A sites.

(B) Validation of subcellular fractionation using RT-qPCR to detect RNAs enriched in the three distinct subcellular fractions. Unspliced *Ccbe1* pre-mRNA is enriched in the CA-RNA fraction. *Neat1* is enriched in both nuclear and CA RNA fractions. The *Actb* mRNA is enriched in both cytoplasmic and nuclear fractions. Mean ± SEM is shown from two biological replicates. Statistical significance calculated using a *Welch's* t-test; * $p \leq 0.05$, ** $p \leq 0.01$, *** $p \leq 1.0 \times 10^{-3}$, **** $p \leq 1.0 \times 10^{-4}$.

(C) Western blot validating subcellular fractionation efficiency in cytoplasmic, nuclear, and chromatin-associated fractions in HEK293T (left), mHippoE-2 (middle), and SH-SY5Y cells (right).

(D) Proportion of reads from DART-seq datasets mapping to intronic and coding regions. Datasets from chromatin-associated (CA), nuclear (Nuc), and cytoplasmic (Cyto) RNA fractions from HEK293T and mHippoE-2 cells are shown.

(E) Distribution of m^{6}A sites identified by DART-seq in cytoplasmic, nuclear, and chromatin-associated RNA fractions from mHippoE-2 and HEK293T cells.

(F) Top ranked motifs enriched near m^{6}A sites identified by DART-seq in the indicated RNA fractions in mHippoE-2 and HEK293T cells.

(G) Metagene profiles of m^{6}A sites and RBM45 CLIP peaks across intronic regions show a consistent 3` bias for RBM45 CLIP peaks and m^{6}A sites identified by DART-seq. Shuffled regions are shown as controls.

Supplemental Figure 4

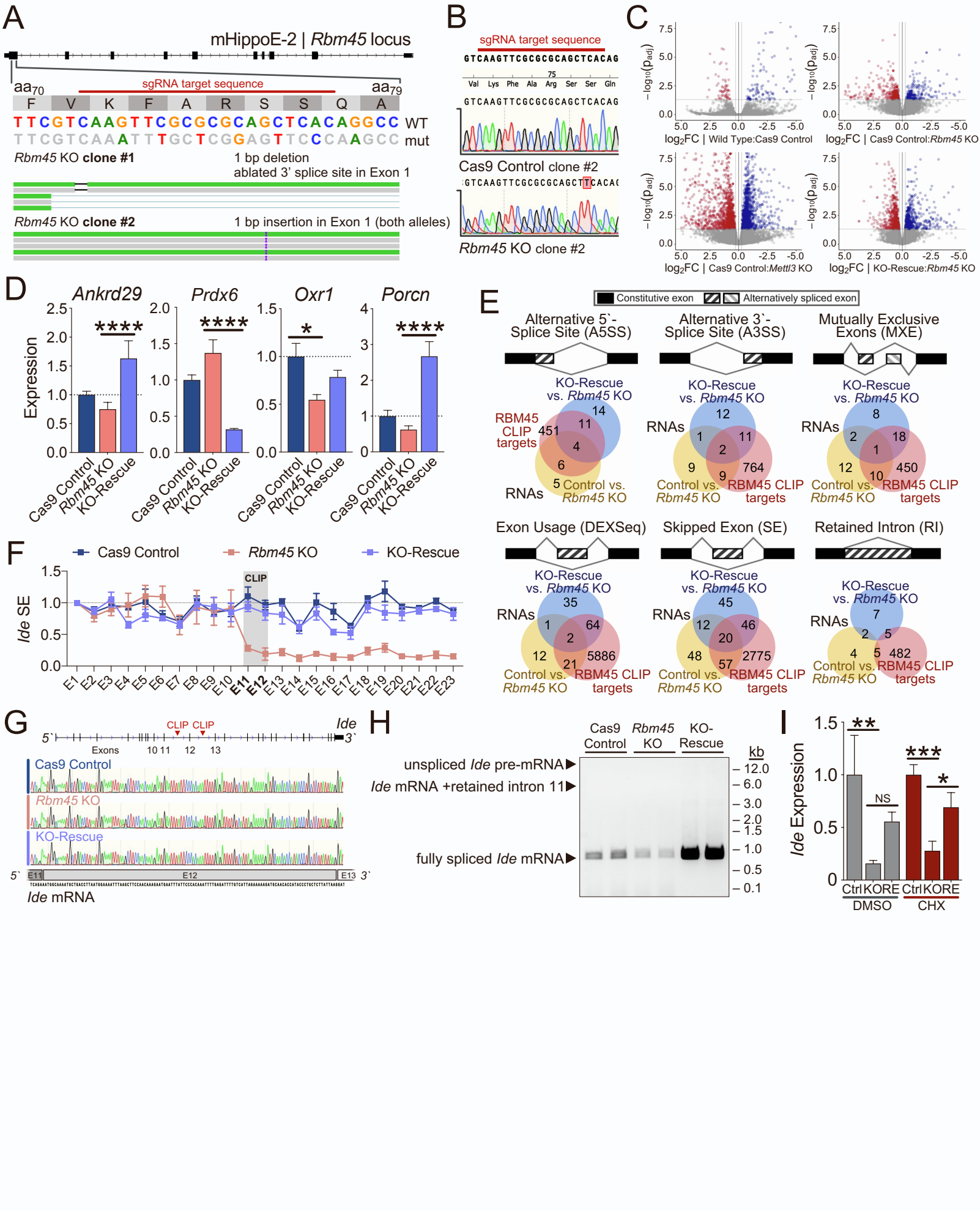

Supplementary Figure 4. Effects of RBM45 depletion in mHippoE-2 stable cell lines.

Related to Figure 3.

(A) Validation of disruption of the *Rbm45* locus in two clonal *Rbm45* KO stable cell lines. mHippoE-2 *Rbm45* KO clone #1 has a 1 bp deletion on one allele, and an ablated 3` splice site at the 3` end of exon 1 on the other allele. mHippoE-2 *Rbm45* KO clone #2 contains a 1 bp insertion on both alleles. Degenerate codon mutations that were introduced in the FLAG-HA-tagged RBM45 rescue sequence to avoid gRNA targeting are indicated below the wild-type sequence (mut and WT, respectively).

(B) Sanger sequencing traces from representative Cas9 Control and *Rbm45* KO mHippoE-2 clonal stable cell lines, revealing the 1 bp deletion in Exon 1 of the Rbm45 coding sequence, which is expected to cause a frameshift mutation.

(C) Scatterplot showing differential gene expression changes (log_2FC, $p_{adj} \leq 0.05$) between Cas9 Control and *Rbm45* KO mHippoE-2 cells (x-axis) and *Rbm45* KO and KO-Rescue mHippoE-2 cells (y-axis). Upregulated RNAs differentially expressed in an RBM45-dependent manner are colored in blue, downregulated differentially expressed in an RBM45-dependent manner are colored in red, and changes not statistically significant (NS) are colored in gray. *Rbm45* and three RBM45-regulated target RNAs chosen for validation are labeled.

(D) RT-qPCR validation of RNA abundance changes across mHippoE-2 Cas9 Control, *Rbm45* KO, and KO-Rescue stable cell lines for high-confidence RBM45 CLIP targets *Ankrd29*, *Neat1*, *Oxr1*, and *Porcn*. Mean ± SEM from 4 biological replicates is shown. Statistical significance calculated using a *Welch's* t-test adjusted for multiple comparisons (Holm-Sidak); * $p \leq 0.05$, ** $p \leq 0.01$, *** $p \leq 1.0 \times 10^{-3}$, **** $p \leq 1.0 \times 10^{-4}$.

(E) Venn diagrams showing genes identified as undergoing alternative splicing when comparing the indicated mHippoE-2 cell lines using two alternative splicing-focused platforms (DEXSeq and rMATS). Few genes exhibit RBM45-dependent alternative splicing, and of these only a small number are CLIP targets.

(F) Splicing efficiency percentage measurements (SE, %) of exons in the *Ide* gene across Cas9 Control, *Rbm45* KO, and KO-Rescue mHippoE-2 stable cell lines. SE percentages downstream of Exon 10 drop sharply in RBM45-depleted cells.

(G) RT-PCR for mature *Ide* mRNA in mHiPPoE-2 stable cell lines following oligo(dT)-primed cDNA synthesis. Predicted products for unspliced and spliced *Ide* mRNAs containing a retained intron 11 are indicated and are not observed in any of the mHiPPoE-2 stable cell lines. Data are representative of three biological replicates.

(H) Sanger sequencing traces are shown across a portion of the *Ide* mRNA coding sequence (Exon 11 to Exon 13) which spans the RBM45 binding sites in introns 11 and 12. Traces for mHippoE-2 Cas9 Control, *Rbm45* KO, and KO-Rescue stable cell lines reveal no differences in the *Ide* mRNA sequence across the cell lines. Sanger sequencing was performed following oligo(dT)-primed RT-PCR.

(I) RT-qPCR expression measurements of *Ide* relative to 18s rRNA in mHippoE-2 stable cell lines with or without inhibition of nonsense-mediated decay (NMD) using cycloheximide (CHX). Mean ± SEM from three biological replicates is plotted. Statistical significance was calculated using *Welch's* t-test.

Supplemental Figure 5

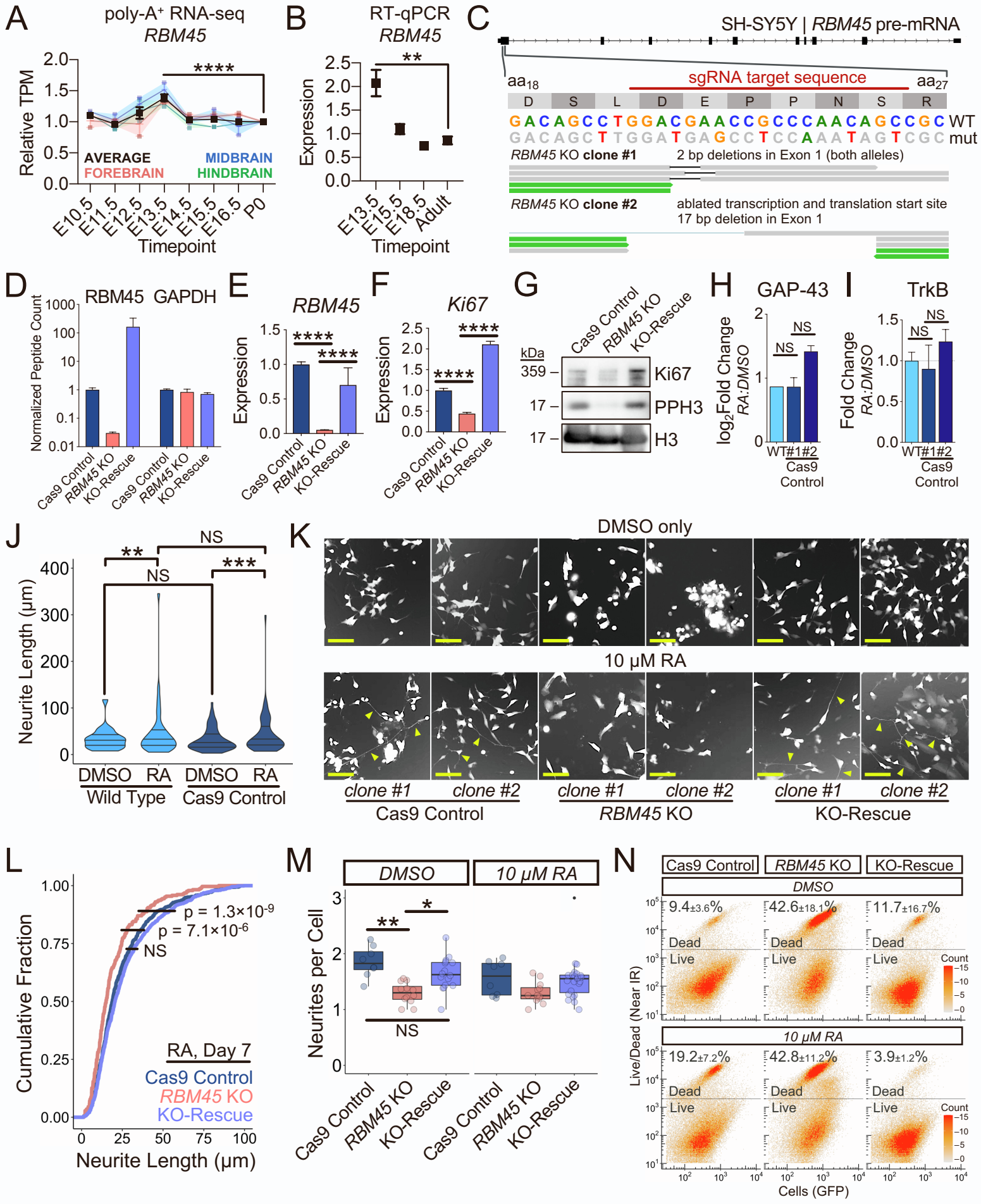

Supplementary Figure 5. RBM45 is necessary for differentiation of SH-SY5Y neuroblastoma cells.

Related to Figure 4.

(A) Expression levels of *Rbm45* mRNA during embryonic development in the mouse brain. TPM counts (transcripts per million bases) were normalized to postnatal day 0 (P0) levels. Mean ± SEM is plotted for total brain expression levels at each timepoint (forebrain, n=2; midbrain, n=2; hindbrain, n=2). Data were mined from the ENCODE development series database: forebrain (ENCSR443OEA), midbrain (ENCSR505AHT), and hindbrain (ENCSR328UYN). Statistical significance calculated using two-way ANOVA with Tukey correction for multiple comparisons; **** $p \leq 1.0 \times 10^{-4}$.

(B) Relative expression of *Rbm45* mRNA determine by RT-qPCR from whole mouse brain RNA at the indicated timepoints during embryonic development. Mean ± SEM is plotted, normalized to relative expression levels of adult mice (≥ 6 weeks old). Statistical significance calculated using two-way ANOVA with Tukey correction for multiple comparisons; ** $p = 1.9 \times 10^{-3}$.

(C) Alignments of RNA-seq data from independent clonal SH-SY5Y stable cell lines at the *RBM45* locus. *RBM45* KO clone #1 contains two distinct 2 bp indels, one on each allele. *RBM45* KO clone #2 contains a 17 bp indel on one allele and an ablated transcription and translation start site on the second allele. Degenerate codon mutations in the FLAG-HA-tagged RBM45 sequence used to make KO-Rescue cell lines is shown relative to the wild type sequence (mut and WT, respectively).

(D) RBM45 and GAPDH protein levels in Cas9 Control, *RBM45* KO, and KO-Rescue SH-SY5Y stable cell lines measured using quantitative mass spectrometry. Mean peptide counts ± SEM are plotted from two clonal cell lines for each genotype and normalized to Cas9 Control cells.

(E) Relative expression of *RBM45* mRNA using RT-qPCR in SH-SY5Y stable cell lines. Mean ± SEM from three biological replicates is shown. Statistical significance calculated using a *Welch's* t-test: **** $p < 1.0 \times 10^{-4}$.

(F) Relative expression of *Ki67* mRNA using RT-qPCR in SH-SY5Y stable cell lines. Mean ± SEM from three biological replicates is shown. Statistical significance calculated using a *Welch's* t-test: **** $p < 1.0 \times 10^{-4}$.

(G) Western blot for proliferation markers Ki67 and phospho-Histone 3 (PPH3) in Cas9 Control, *RBM45* KO, and KO-Rescue SH-SY5Y stable cell lines. Data are representative of six biological replicates. Histone H3 levels are shown as a control.

(H) Quantification of GAP-43 protein expression for wild type (WT) and Cas9 Control SH-SY5Y stable cell lines in response to differentiation with 10 µM RA. Log_2 fold change of ratio between RA-treated and DMSO-treated cells is shown. Mean ± SEM for western blot protein band intensity was normalized to total protein (Coomassie) and/or housekeeping gene marker (GAPDH, Histone 3) levels. Statistical significance was calculated using a *Welch's* t-test; ns, $p > 0.05$.

(I) Quantification of NTRK2 protein expression for wild type (WT) and Cas9 Control SH-SY5Y stable cell lines in response to differentiation with 10 µM RA. Log_2 fold change of ratio between RA-treated and DMSO-treated cells is shown. Mean ± SEM for western blot protein band intensity was normalized to total protein (Coomassie) and/or housekeeping gene marker (GAPDH, Histone 3) levels. Statistical significance was calculated using a *Welch's* t-test; ns, $p > 0.05$.

(J) Violin plots showing the distribution of neurite lengths for WT and Cas9 Control SH-SY5Y stable cell lines after 7 days of treatment with DMSO or 10 µM RA. Distributions, medians, and quartiles of neurite length (µm) from multiple biological replicates is plotted. Statistical significance determined using Kolmogorov-Smirnov (K-S) test; p-values from left to right: ** $p = 6.2 \times 10^{-3}$, *** $p = 8.7 \times 10^{-4}$.

(K) Representative images of Cas9 Control, *RBM45* KO, and KO-Rescue SH-SY5Y stable cell lines treated with DMSO or 10 µM RA for 7 days. Yellow arrows indicate extended neurites. Yellow scale bar=50 µm.

(L) Cumulative distribution plots of neurite length for SH-SY5Y Cas9 Control, *RBM45* KO, and KO-Rescue cell lines after 7 days of treatment with 10 µM RA. *RBM45* KO cells have a larger fraction of shorter neurites following RA treatment compared to Cas9 Control and KO-Rescue cells. (Cas9 Control vs. *RBM45* KO: ****p= 1.3×10-9; *RBM45* KO vs. *RBM45* KO Rescue: ****p=7.1×10-6). Statistical significance tested using Kolmogorov-Smirnov (K-S) test.

(M) Boxplots showing number of neurites per cell from SH-SY5Y stable cell lines following treatment with either DMSO or 10 µM RA. Statistical significance determined using Kolmogorov-Smirnov (K-S) test; p-values from left to right: ** $p = 1.3 \times 10^{-3}$, * $p = 4.9 \times 10^{-2}$.

(N) Two-dimensional absorbance plots of SH-SY5Y Control, *RBM45* KO, and KO-Rescue cells subjected to flow cytometry to assess stable cell line viability using a dead-cell permeable near-infrared fluorescent dye. Cells were treated with DMSO or 10 µM RA for 7 days. Mean population of dead cells ± SEM is plotted.

Supplemental Figure 6

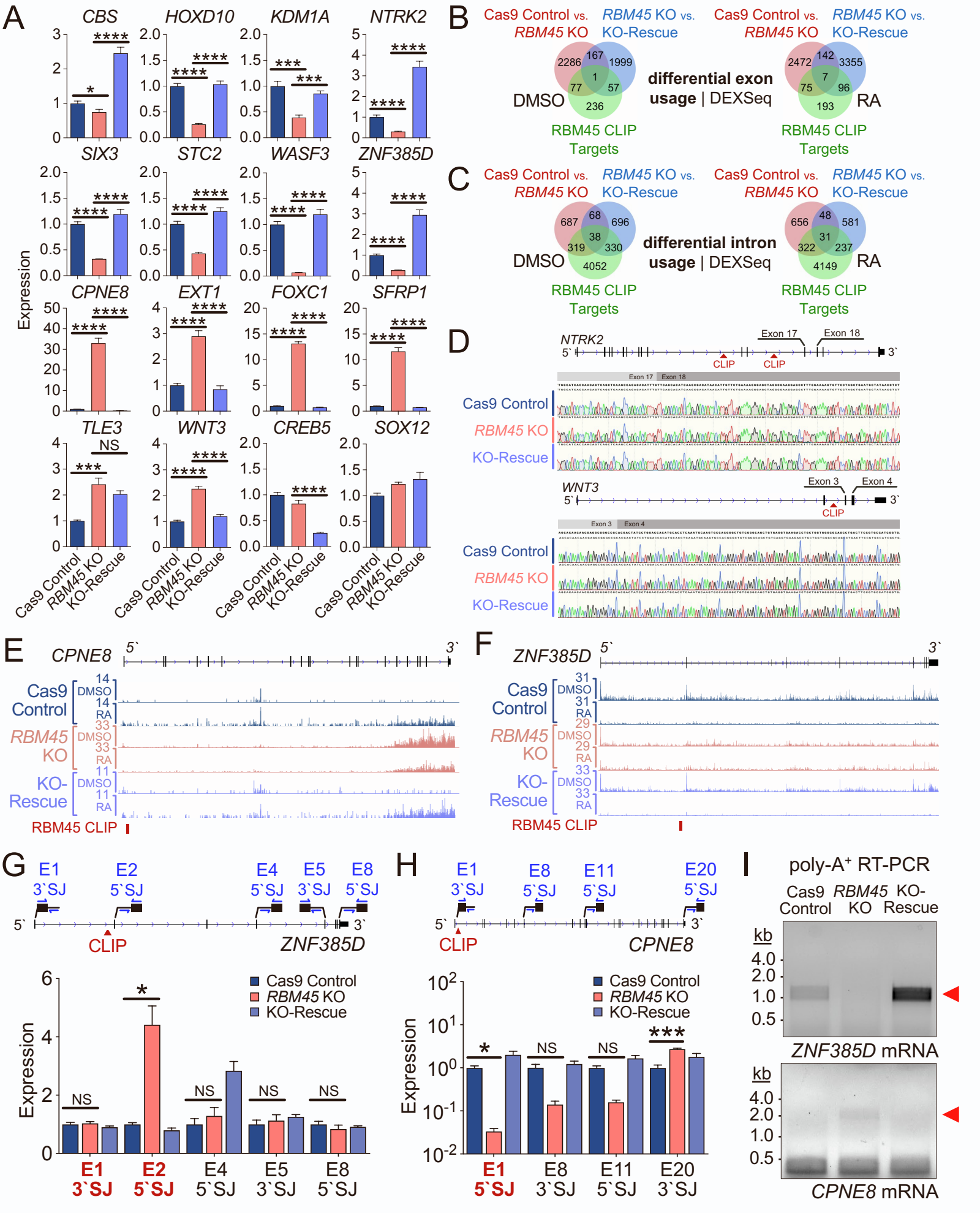

Supplemental Figure 6. Effects of RBM45 on gene expression in SH-SY5Y cells.

Related to Figures 5 & 6.

(A) RT-qPCR showing relative expression levels of RBM45 target mRNAs in undifferentiated Cas9 Control, *RBM45* KO, and KO-Rescue stable cell lines. 14 of 16 selected targets selected from RNA-seq data were validated using RT-qPCR. Mean ± SEM from three biological replicates is shown. Statistical significance calculated using a *Welch's* t-test adjusted for multiple comparisons (Holm-Sidak); * $p \leq 0.05$, ** $p \leq 0.01$, *** $p \leq 1.0 \times 10^{-3}$, **** $p \leq 1.0 \times 10^{-4}$.

(B) Venn Diagrams showing RNAs with significant differential exon usage changes between 1) Cas9 Control and *RBM45* KO cells and 2) *RBM45* KO and KO-Rescue cells after DMSO (left) or RA treatment (right). CLIP target RNAs are also shown. Only 1 RNA bearing RBM45-dependent differential exon usage events was a CLIP target in DMSO-treated cells, and 7 RNAs were identified as CLIP targets in RA-treated cells.

(C) Venn Diagrams showing RNAs with significant differential intron usage changes between 1) Cas9 Control and *RBM45* KO cells and 2) *RBM45* KO and KO-Rescue cells after DMSO (left) or RA treatment (right). CLIP target RNAs are also shown. 38 RNAs bearing RBM45-dependent differential intron usage events were CLIP targets in DMSO-treated cells, and 31 RNAs were identified as CLIP targets in RA-treated cells.

(D) Sanger sequencing traces are shown across a portion of the *NTRK2* and *WNT3* mRNA coding sequences. Traces for Cas9 Control, *RBM45* KO, and KO-Rescue SH-SY5Y stable cell lines reveal no differences in either *NTRK2* or *WNT3* mRNA coding sequences. Sanger sequencing was performed following oligo(dT)-primed RT-PCR.

(E) Representative alignments of Cas9 Control, *RBM45* KO, and KO-Rescue SH-SY5Y stable cell lines for the *CPNE8* transcript, with RBM45 CLIP peak regions shown below alignments.

(F) Representative alignments of Cas9 Control, *RBM45* KO, and KO-Rescue SH-SY5Y stable cell lines for the *ZNF385D* transcript, with RBM45 CLIP peak regions shown below alignments.

(G) Relative expression measurements of exon-intron junctions along the *ZNF385D* pre-mRNA. Primer pairs target the indicated 5`- or 3`-splice junctions (SJ's). Exon-intron junctions flanking RBM45 target introns are labeled in red in the bar graph. Mean ± SEM from three biological replicates is shown. Statistical significance was calculated using a *Welch's* t-test adjusted for multiple comparisons (Holm-Sidak), adjusted p-values: ** $p = 6.9 \times 10^{-3}$.

(H) Relative expression measurements of exon-intron junctions along the *CPNE8* pre-mRNA. Primer pairs target the indicated 5`- or 3`-splice junctions (SJ's). Exon-intron junctions flanking RBM45 target introns are labeled in red in the bar graph. Mean ± SEM from three biological replicates is shown. Statistical significance was calculated using a *Welch's* t-test adjusted for multiple comparisons (Holm-Sidak), adjusted p-values (p_{adj}) shown; * $p \leq 0.05$, ** $p \leq 0.01$, *** $p \leq 1.0 \times 10^{-3}$, **** $p \leq 1.0 \times 10^{-4}$.

(I) RT-PCR for mature *ZNF385D* (top) and *CPNE8* (bottom) mRNAs in SH-SY5Y stable cell lines using oligo(dT)-primed cDNA indicates no evidence of products with retained introns in any of the stable cell lines. Arrowheads indicate the predicted size of mature, spliced mRNA. Data are representative of three biological replicates.

Supplemental Figure 7

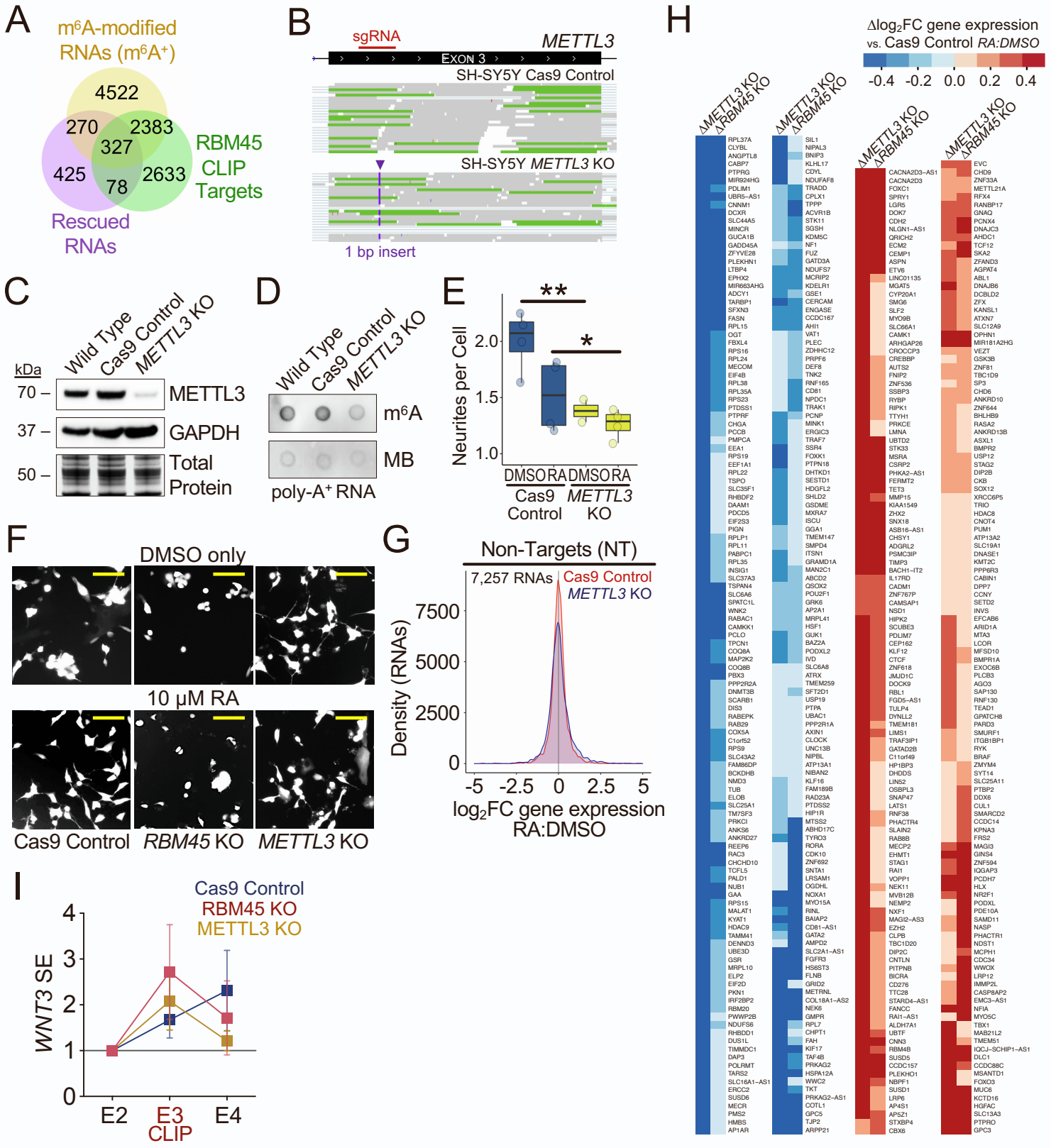

Supplemental Figure 7. Effects of METTL3 depletion in SH-SY5Y cells.

Related to Figure 7.

(A) Venn diagram showing overlap among RNAs that are differentially expressed after RA treatment in Cas9 Control and KO-Rescue SH-SY5Y cells (RA:DMSO $p_{adj} \leq 0.05$, purple), m^6A-modified RNAs expressed in SH-SY5Y cells (m^6A^+ $p_{adj} \leq 1$, yellow), and RBM45 CLIP target RNAs expressed in SH-SY5Y cells (CLIP, green). 195 of 412 (47.3%) differentially expressed target RNAs contain overlapping CLIP peaks and m^6A sites.

(B) Gene tracks showing RNA-seq reads from Cas9 Control and *METTL3* KO SH-SY5Y stable cell lines at exon 3 of the *METTL3* locus. *METTL3* KO cells have a 1 bp insertion in the coding sequence on both alleles, resulting in a predicted frameshift mutation.

(C) Western blot showing METTL3 expression in wild type, Cas9 Control, and *METTL3* KO SH-SY5Y stable cell lines. Data are representative of three biological replicates. GAPDH expression and total protein are shown as loading controls.

(D) Dot blot for m^6A using 100 ng of poly(A)-purified RNA isolated from wild type, Cas9 Control, and *METTL3* KO SHSY5Y stable cells. Methylene Blue stain (MB) is shown as a loading control.

(E) Boxplots of neurites per cell in DMSO-treated and RA-treated Cas9 Control and *METTL3* KO SH-SY5Y stable cells. Distributions, medians, and quartiles of the number of neurites per cell from multiple biological replicates is plotted. Statistical significance determined using Kolmogorov-Smirnov (K-S) test; p-values from left to right: ** $p=1.3\times10^{-3}$, * $p=4.9\times10^{-2}$.

(F) Images of Cas9 Control, *RBM45* KO, and *METTL3* KO SH-SY5Y cells treated with DMSO or RA for 7 days. Yellow scale bar=50 µm.

(G) Gene expression response to RA treatment for 11,365 RNAs that are not RBM45 CLIP targets (NT RNAs). Only RNAs with sufficient coverage in the cell lines are shown. Similar gene expression responses of NT RNAs are observed in Cas9 Control and *METTL3* KO cells.

(H) Clustered heat maps of 514 RNAs that are differentially expressed after RA treatment in SH-SY5Y Cas9 Control cells ($p_{adj} \leq 0.05$) and co-regulated by METTL3 and RBM45. The change in $\log_2$FC gene expression between Cas9 Control and *METTL3* KO or *RBM45* KO stable cell lines ($\Delta\log_2FC = \log_2FC\ \text{Cas9 Control}_{RA:DMSO} - \log_2FC\ \textit{METTL3}/\textit{RBM45}\ \text{KO}_{RA:DMSO}$) are plotted, with gene names labeled.

(I) Splicing efficiency (SE) measurements of exon inclusion in *WNT3* using bipartite reads from RNA-seq data from the indicated SH-SY5Y stable cell lines. Shown are the levels of exon inclusion relative to the first exon.